Inorganic Chemistry

Article

pubs.acs.org/IC

Immobilization of Ultrafine Bimetallic Ni–Pt Nanoparticles Inside the Pores of Metal–Organic Frameworks as Efficient Catalysts for Dehydrogenation of Alkaline Solution of Hydrazine

Nan Cao,[†] Lan Yang,[†] Hongmei Dai,[†] Teng Liu,[†] Jun Su,[†,§] Xiaojun Wu,[†] Wei Luo,*[,†,‡] and Gongzhen Cheng[†]

[†]College of Chemistry and Molecular Sciences, Wuhan University, Wuhan, Hubei 430072, P. R. China

[‡]Suzhou Institute of Wuhan University Suzhou, Wuhan, Jiangsu 215123, P. R. China

[§]Wuhan National Laboratory for Optoelectronics, Huazhong University of Science and Technology, Wuhan University, Wuhan, Hubei 430074, P. R. China

ABSTRACT: We report a facile liquid impregnation approach for immobilization of ultrafine bimetallic Ni–Pt nanoparticles (NPs) inside the pores of MIL-101. The methods of powder X-ray diffraction, N_2 physisorption, X-ray photoelectron spectroscopy, transmission electron microscopy, and inductively coupled plasma-atomic emission spectroscopy were employed to characterize the NiPt@MIL-101 catalysts and further indicated the as-synthesized Ni–Pt NPs were confined in the pores of MIL-101. These as-synthesized bimetallic NiPt@MIL-101 NPs exhibit exceedingly high catalytic activity, selectivity, and durability toward hydrogen generation from alkaline solution of hydrazine.

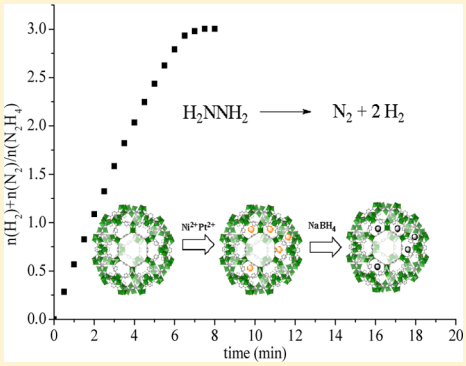

1. INTRODUCTION

The synthesis of metal nanoparticles (NPs) with controllable size and distribution has attracted growing attention owing to the unique properties and potential applications of NPs.[1−3] Heterogeneous catalysis is one of the most important applications of metal NPs.[4−7] Their catalytic performance is highly dependent on the dispersion of active metal sites; therefore, many techniques have been designed to avoid the aggregation during their synthesis route.[8−10] Among them, stabilizing NPs in the matrices of solid materials is one of most common and efficient ways to prevent aggregation. Until now, a number of porous materials such as zeolite,[11] metal oxide,[12] polymers,[13] carbon nanotube,[14] and graphene[15] have been designed for restraining the aggregation of metal NPs. Metal–organic frameworks (MOFs) have been emerging as a class of promising porous functional materials owing to their high porosity, large surface area, chemical tunability and thus specific applications, such as gas sorption and storage,[16,17] molecular recognition, and separation,[18,19] drug delivery,[20,21] luminescence,[22,23] magnetic properties,[24,25] and catalytic properties.[26,27] Given the similarity to zeolites, loading metal NPs into the pores of MOFs is expected to control the limited growth of metal NPs in the confined cavities and produce monodispersed NPs, which could further increase their catalytic activities.[28] Moreover, the three-dimensional pore structures, presence of organic linkers, and chemical tunabilities make MOFs possess unique advantages over other porous materials.[29−31] However, up to now, reports about MOF-supported metal NPs were mainly focused on monometallic systems,[32] while the bimetallic NPs supported on MOFs with more obvious synergistic effect, to the best of our knowledge, have not been widely studied.[33,34]

On the other hand, hydrogen is a globally accepted clean fuel due to its high efficiency and power density. The development of safe and efficient hydrogen storage materials still remains one of the most challenging barriers for establishing a future hydrogen economy.[35] Over the past decades, there has been rapidly growing interest for searching suitable hydrogen storage materials including metal hydride,[36] sorbent materials,[37,38] and chemical hydride systems.[39,40] Among the chemical hydrogen storage materials, hydrazine monohydrate ($N_2H_4{\cdot}H_2O$) was developed as a promising hydrogen carrier due to its high hydrogen content (8.0 wt %) and easy recharging property.[41−44] Moreover, hydrazine monohydrate is a liquid-phase material which has the potential to take the advantage of the exiting liquid-based distribution infrastructure, which makes hydrazine monohydrate more competitive than the solid chemical hydrogen storage materials such as sodium borohydride ($NaBH_4$) and ammonia borane (NH_3BH_3) derivatives. The decomposition of hydrazine proceeds via two competitive routes:

$$H_2NNH_2(aq) \rightarrow N_2(g) + 2H_2(g) \quad (1)$$

Received: May 3, 2014
Published: September 8, 2014

dx.doi.org/10.1021/ic5010352 | Inorg. Chem. 2014, 53, 10122−10128

$$3H_2NNH_2(aq) \rightarrow N_2(g) + 4NH_3(g) \quad (2)$$

From the perspective of hydrogen storage application, the undesired reaction route 2 should be avoided. Thereby, it is a great challenge to develop efficient catalysts with high selectivity. To this end, a number of noble, non-noble metal-containing mono- and bimetallic nanocatalysts have been recently developed.[45−54] However, finding the optimal compromise between costs, selectivity, efficiency, and recyclability still remains a considerable challenge.

Herein, we report the preparation and characterization of MIL-101-supported bimetallic Ni−Pt NPs and the application of these NPs in the dehydrogenation of alkaline solution of hydrazine. Our study found that the NiPt@MIL-101 catalyst synergistically improves the catalytic activity compared with their monometallic MIL-101 supported NPs and alloy NPs without MIL-101 support. MIL-101, a chromium-based MOF, $Cr_3F(H_2O)_2O[(O_2C)C_6H_4(CO_2)]_3{\cdot}nH_2O$ ($n \approx 25$) was selected due to its extra-high specific surface area, its pore volume, and its high thermal (up to 300 °C) and good chemical resistance to water.[55]

2. RESULTS AND DISCUSSION

MIL-101 was synthesized according to the literature,[55] followed by treatment with EtOH and aqueous NH_4F solution to remove the unreacted terephthalic acid. As shown in Scheme 1, activated MIL-101 was impregnated with deionized water containing $NiCl_2$ and K_2PtCl_6 in 98:2, 95:5, 90:10, 70:30, and 30:70 molar ratio at 25 °C for 8 h. The suspension was separated by centrifugation, and after reduced by sodium borohydride, the as-synthesized NiPt@MIL-101 catalysts with different Ni/Pt compositions were obtained. The final ratio of Ni and Pt in the catalysts were determined by the inductively coupled plasma atomic emission spectroscopic (ICP-AES), which were very close to the initial loading (Table 1). There was no apparent loss of crystallinity from the low-angle powder X-ray diffraction (PXRD) patterns of all NiPt@MIL-101 samples compared with parent MIL-101 (Figure 1a), suggesting that the integrity of the MIL-101 framework was maintained well. Furthermore, from the wide-angle PXRD (Figure 1b), the diffraction peak of NiPt@MIL-101 is different from the Pt (111) (39.2°), Pt (200) (46.0°), and the Ni (111) (44.3°), indicating the formation of Ni−Pt alloy.

Scheme 1. Synthesis of NiPt@MIL-101 Nanocatalysts

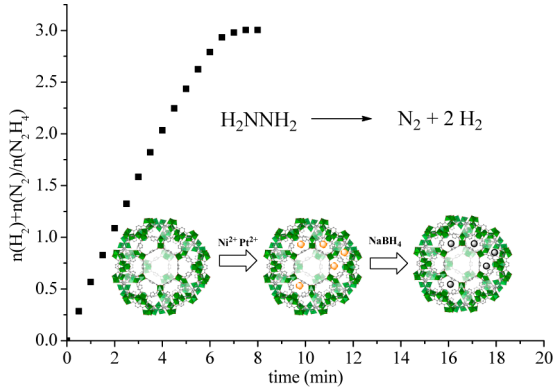

The surface area of $Ni_{88}Pt_{12}$@MIL-101 was calculated from the N_2 isotherm using the BET model (Figure 2). In comparison with that of MIL-101, the obvious decrease in the amount of N_2 adsorption and the pore volume (Table 2) of $Ni_{88}Pt_{12}$@MIL-101 indicates that the cavities of the host framework are either occupied by the dispersed NiPt NPs or blocked by the NiPt NPs.[56] The X-ray photoelectron spectroscopy (XPS) of $Ni_{88}Pt_{12}$@MIL-101 (Figure 3) exhibit characteristic signals for Ni^0 and Pt^0, indicating the coexistence of both metals. The formation of oxidized Ni observed at 856.5 and 874.9 eV most likely occurs during the sample preparation process for the XPS measurements.[48,57]

The microstructure of $Ni_{88}Pt_{12}$@MIL-101 was further characterized by transmission electron microscopic (TEM) and energy dispersive X-ray spectrometry (EDX). As shown in Figure 4a, the well-dispersed NiPt NPs with an average diameter of 1.8 ± 0.4 nm were observed, indicating that the NiPt NPs are small enough to be accommodated into the two mesoporous cavities of MIL-101 (2.9 and 3.4 nm) and big enough to be limited in the pores of the framework by the windows of MIL-101 (1.2 and 1.6 nm), which helps to prevent the agglomeration of NPs. In Figure 4c, the *d*-spacing of the NPs is ∼0.225 nm, which differing from the Pt (111) crystal plane (0.227 nm) and the Ni (111) plane (0.204 nm), further demonstrating the crystalline nature of Ni−Pt alloy NPs. The EDX spectra further confirm the presence of NiPt.

The as-synthesized NiPt@MIL-101 NPs with different composition have been tested for the catalytic dehydrogenation of aqueous solution of hydrazine at 50 °C in the presence of NaOH (0.5 M) as shown in Figure 5. The activity of the catalysts was strongly dependent on the Ni−Pt composition, while Ni@MIL-101 is almost catalytic inactive, showing a poor catalytic activity (only about 1.5 equiv of gas was released over 3 h) and low hydrogen selectivity (53.8%). By alloying Pt to Ni, the catalytic activity and selectivity of the catalysts increased obviously. $Ni_{88}Pt_{12}$@MIL-101 exhibits the highest catalytic activity, with the turnover frequency (TOF) value of 375.1 h^{-1} at 50 °C, which is the highest among all the reported catalysts (Table 3). The H_2 selectivity and completeness of hydrazine decomposition over $Ni_{88}Pt_{12}$@MIL-101 are further confirmed by mass spectroscopy (Figure 6), indicating the 100% H_2 selectivity. Further increased Pt ratio results in the lower catalytic activity as shown in $Ni_{68}Pt_{32}$@MIL-101, with the TOF value of 276.3 h^{-1}. When Pt increased to 72% in $Ni_{28}Pt_{72}$@MIL-101, a much poor catalytic (only about 1.5 equiv of gas was released over 1 h) and lower hydrogen selectivity (52.2%) were observed. Even worse, no hydrogen was released on monometallic Pt@MIL-101, revealing the positive effect of metal interaction in the as-synthesized Ni−Pt alloy NPs on

Table 1. ICP-AES Results of Different Catalysts

catalyst	$Ni_{97}Pt_3$	$Ni_{94}Pt_6$	$Ni_{88}Pt_{12}$	$Ni_{67}Pt_{33}$	$Ni_{28}Pt_{72}$
Ni−Pt initial composition	$Ni_{98}Pt_2$	$Ni_{95}Pt_5$	$Ni_{90}Pt_{10}$	$Ni_{70}Pt_{30}$	$Ni_{30}Pt_{70}$
Ni (wt %)	3.07	3.83	4.53	3.35	1.83
Pt (wt %)	0.29	0.77	2.00	5.17	15.85
final metals/catalyst (mmol/100 mg)	0.054	0.069	0.087	0.084	0.112

dx.doi.org/10.1021/ic5010352 | Inorg. Chem. 2014, 53, 10122−10128

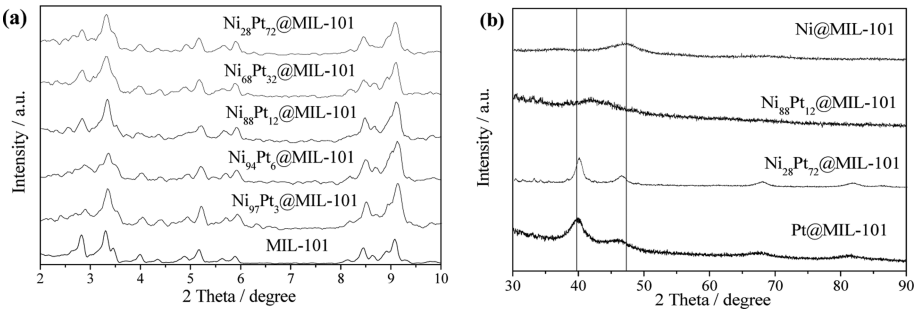

Figure 1. (a) Powder X-ray diffraction patterns of samples. (b)The wide-angle PXRD of Ni@MIL-101, $Ni_{88}Pt_{12}$@MIL-101, $Ni_{28}Pt_{72}$@MIL-101, and Pt@MIL-101.

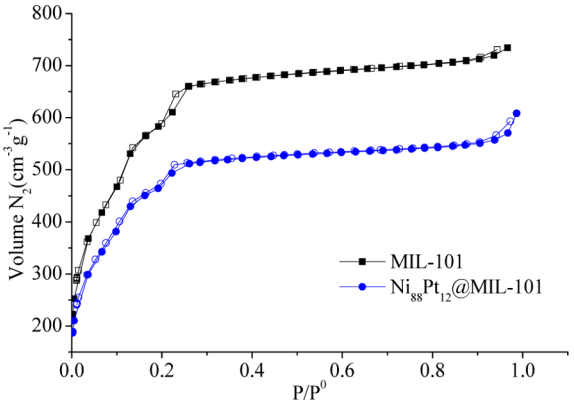

Figure 2. N_2 sorption isotherms of activated MIL-101 and $Ni_{88}Pt_{12}$@MIL-101 at 77 K. Filled and open symbols represent adsorption and desorption branches, respectively.

Table 2. Pore Volume and Surface Area of MIL-101 and $Ni_{88}Pt_{12}$@MIL-101

sample	wt %	surface area (m^2 g^{-1})	pore volume (m^3 g^{-1})
MIL-101		2233	1.195
$Ni_{88}Pt_{12}$@MIL-101	6.53	1772	0.941

hydrogen generation and selectivity. Furthermore, as a control experiment, the same amount of $Ni_{88}Pt_{12}$ NPs, the physical mixture of Pt@MIL-101 and Ni@MIL-101 with a molar ratio of 12/88, $Ni_{88}Pt_{12}$@MIL-101 after 1 d of exposure to air, and MIL-101 were synthesized and applied to dehydrogenation of alkaline solution of hydrazine. As shown in Figure 7, only 2.5 equiv of gas with 82.1% hydrogen selectivity were released for more than 35 min for $Ni_{88}Pt_{12}$ NPs, and almost no reactivity for MIL-101 toward hydrolysis of alkaline solution of hydrazine at 50 °C. These results confirm the synergistic effect of NiPt NPs and framework of MIL-101. The physical mixing Pt@MIL-101 to Ni@MIL-101 does not give significant efforts to the catalytic activity, indicating the synergistic effect of Ni and Pt in the same materials is the key for enhancing their catalytic activities.[48] In addition, there is an obvious decrease in the catalytic activity of $Ni_{88}Pt_{12}$@MIL-101 after 1 d of exposure to air, but the H_2 selectivity was not changed. This result may be caused by large H_2 generation and the M−H species during the catalytic process which could further reduce the oxidized Ni to Ni(0).

To obtain the activation energy (E_a) of the dehydrogenation of alkaline solution of hydrazine catalyzed by $Ni_{88}Pt_{12}$@MIL-101, the catalytic experiments were carried out at temperatures ranging from 25 to 60 °C (Figure 8), and E_a was determined to be 51.29 kJ mol^{-1}, which is close to the reported values (Table 3). Furthermore, the TOF value of the $Ni_{88}Pt_{12}$@MIL-101 at 25 °C was 65.2 h^{-1}, which is among the highest values at 25 °C ever reported (Table 3). In addition, the as-synthesized $Ni_{97}Pt_3$@MIL-101, and $Ni_{88}Pt_{12}$@MIL-101 were tested in terms of durability in five cyclic usages. As shown in Figure 9, there was a slight decrease of activity after five cycles, but the hydrogen selectivity was not changed.

3. CONCLUSION

In summary, we have developed a highly efficient heterogeneous catalyst system for dehydrogenation of alkaline solution of hydrazine using MIL-101 supported bimetallic Ni−Pt alloy NPs as catalyst. The well-dispersed Ni−Pt NPs have been successfully immobilized by the framework of MIL-101, which exhibits the highest catalytic activity toward dehydrogenation of alkaline solution of hydrazine up to now. The combination of

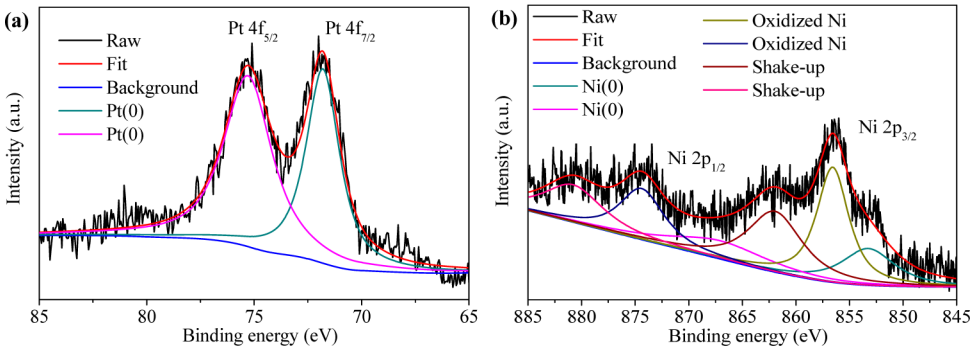

Figure 3. (a) XPS spectra for catalyst NiPt@MIL-101 showing Pt 4f. (b) XPS spectra for catalyst NiPt@MIL-101 showing Ni 2p.

dx.doi.org/10.1021/ic5010352 | Inorg. Chem. 2014, 53, 10122−10128

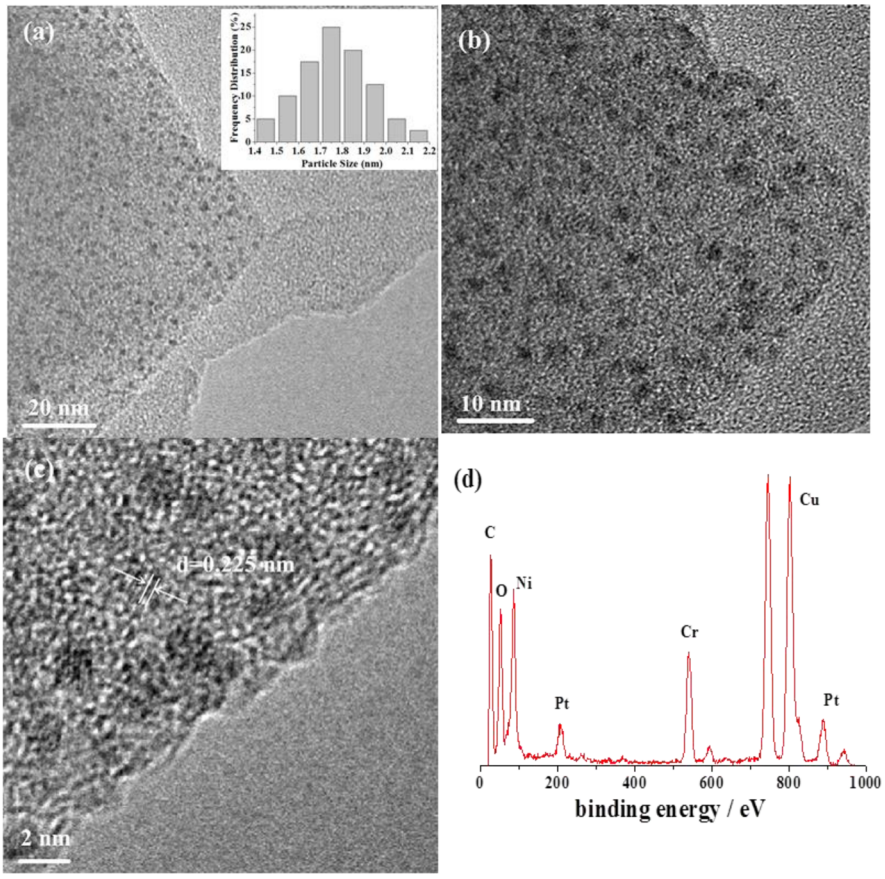

Figure 4. (a–c) TEM images of $Ni_{88}Pt_{12}$@MIL-101with different magnifications. (inset) Particle size distributions of $Ni_{88}Pt_{12}$NPs. (d) EDX of $Ni_{88}Pt_{12}$@MIL-101.

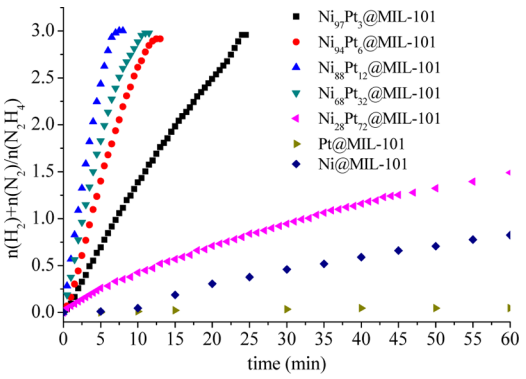

Figure 5. Time course plots for the decomposition of aqueous solution of hydrazine over NiPt@MIL-101 with NaOH (0.5 M) at 50 °C. (catalyst = 0.100 g; $N_2H_4{\cdot}H_2O$ = 0.1 mL).

high activity and selectivity as well as good durability enables NiPt@MIL-101 as a potential catalyst for practical applications in dehydrogenation of alkaline solution of hydrazine for chemical hydrogen storage. Furthermore, this simple synthetic method can be extended to other water-stable MOFs as effective supports to immobilize bimetallic/polymetallic metal NPs for more applications.

4. EXPERIMENTAL SECTION

Chemicals and Materials. All chemicals were commercial and used without further purification. Chromic nitrate nonahydrate ($Cr(NO_3)_3{\cdot}9H_2O$, Sinopharm Chemical Reagent Co., Ltd., 99%), nickel chloride hexahydrate ($NiCl_2{\cdot}6H_2O$, Sinopharm Chemical Reagent Co., Ltd., ≥99%), potassium chloroplatinate (K_2PtCl_6, Wuhan Greatwall Chemical Co., Ltd., 99%), hydrazine monohydrate ($H_4N_2{\cdot}H_2O$, TCI Shanghai Co., Ltd., >98%), aqueous hydrofluoric acid (HF, Sinopharm Chemical Reagent Co., Ltd., 40%), terephthalic acid ($HO_2CC_6H_4CO_2H$, Sinopharm Chemical Reagent Co., Ltd.,

Table 3. Comparison of Activities and E_a of Different Catalysts for Hydrogen Generation by $H_2NNH_2{\cdot}H_2O$ Decomposition

catalyst	T (°C)	TOF (h^{-1})	E_a (kJ/mol)	reference
G4-OH($Pt_{12}Ni_{48}$)	70	240		43
NiFe	70	6.6		49
$Ni_{88}Pt_{12}$@MIL-101	50	375.1	51.29	this study
$Ni_{80}Pt_{20}$@ZIF-8	50	90		34
$Ni_{64.1}Mo_{11.5}B_{24.4}$-La$(OH)_3$	50	13.3	55.1	46
$Ni_{0.99}Pt_{0.01}$	50	6	49.95	58
$Ni_{0.6}Pd_{0.4}$	50	6		52
$Rh_{10}Ni_{90}$	50	4.5		53
Raney Ni-300	30	114	44.4	45
$NiPt_{0.057}/Al_2O_3$	30	16.5	49.3	42
Ni/Al_2O_3	30	2.2	34	42
$Ni_{1.5}Fe_{1.0}$-alloy/$(MgO)_{3.5}$	26	1.9		59
$Ni_{88}Pt_{12}$@MIL-101	25	65.2		this study
$Ni_{0.9}Pt_{0.1}/Ce_2O_3$	25	28.1	42.3	47
Rh_4Ni/graphene	25	20		54
Rh_4Ni	25	9.6		48
$Ni_{0.93}Pt_{0.07}$	25	3		50
Rh	25	2.8		41
$Ni_{0.95}Ir_{0.05}$	25	1.6		60

dx.doi.org/10.1021/ic5010352 | Inorg. Chem. 2014, 53, 10122–10128

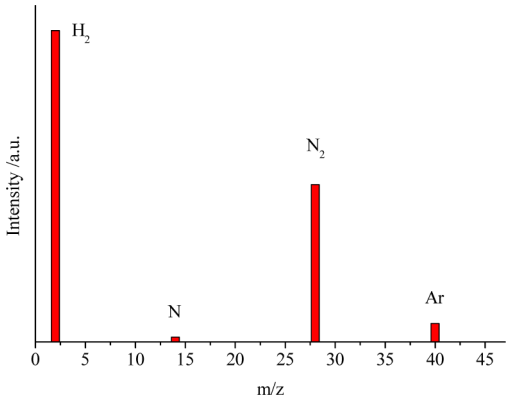

Figure 6. MS profile for the gases released from the decomposition reaction of hydrazine in aqueous NaOH solution (0.5 M) over $Ni_{88}Pt_{12}$@MIL-101 (catalyst = 0.100 g; $N_2H_4{\cdot}H_2O$ = 0.1 mL) under an argon atmosphere at 50 °C.

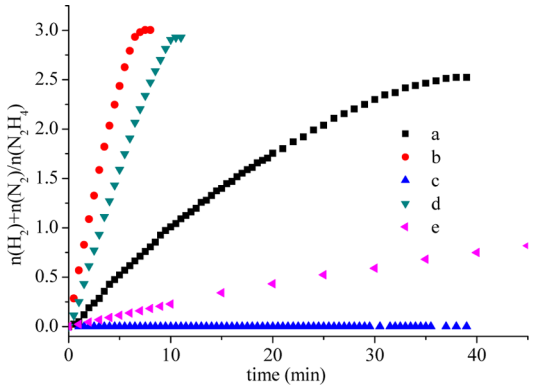

Figure 7. Decomposition of aqueous solution of hydrazine to H_2 over time by (a) $Ni_{88}Pt_{12}$, (b) $Ni_{88}Pt_{12}$@MIL-101, (c) MIL-101, (d) $Ni_{88}Pt_{12}$@MIL-101 exposed in the air for 1 d, and (e) physical mixture of Ni@MIL-101 and Pt@MIL-101 in the presence of NaOH (0.5 M) at 50 °C.

99%), sodium borohydride ($NaBH_4$, Sinopharm Chemical Reagent Co., Ltd., 96%), ammonium fluoride (NH_4F, Sinopharm Chemical Reagent Co., Ltd., ≥96%), ethanol (C_2H_5OH, Sinopharm Chemical Reagent Co., Ltd., >99.8%) were used as received. We use ordinary distilled water as the reaction solvent.

Synthesis of MIL-101. MIL-101 was synthesized using the reported procedure.[52] Terephthalic acid (332 mg, 2.0 mmol), $Cr(NO_3)_3{\cdot}9H_2O$ (800 mg, 2.0 mmol), aqueous HF (0.1 mL, 40 wt %), and deionized water (9.6 mL) were placed in a 50 mL Teflon-liner autoclave and heated at 220 °C for 8h. After natural cooling, the suspension was centrifuged to separate the green powder of MIL-101 with formula $Cr_3F(H_2O)_2O[(O_2C)C_6H_4(CO_2)]_3{\cdot}nH_2O$ ($n \approx 25$), and then further purified by solvothermal treatment in ethanol at 80 °C for 24 h. The resulting green solid was soaked in NH4F (1 M) solution at 70 °C for 24 h to eliminate the terephthalic acid inside the pores of MIL-101 and immediately filtered resulting green solid was finally dried overnight at 150 °C under vacuum for further use.

Synthesis of NiPt@MIL-101. Activated MIL-101 (100 mg) was mixed with 10 mL of deionized water containing 0.02 mmol of K_2PtCl_6 and 0.18 mmol of $NiCl_2{\cdot}6H_2O$, and stirring was continued for 8 h at 25 °C to impregnate the metal salts. After the impregnation, the suspension was separated by centrifugation. The solid was dried at 100 °C and then reduced by sodium borohydride ($NaBH_4$, 37.8 mg) solution with vigorous stirring at 0 °C to yield $Ni_{88}Pt_{12}$@MIL-101. The preparation of the $Ni_{97}Pt_3$@MIL-101, $Ni_{94}Pt_6$@MIL-101, $Ni_{67}Pt_{33}$@MIL-101, $Ni_{28}Pt_{72}$@MIL-101, Pt@MIL-101, and Ni@MIL-101 is following the analogous process.

Decomposition of Aqueous Solution of Hydrazine. In a typical experiment, $Ni_{88}Pt_{12}$@MIL-101(100 mg) and NaOH (80 mg) were dissolved in 4 mL of water kept in a two-necked round-bottom flask with vigorous stirring. One neck was connected to a gas buret to monitor the volume of the gas evolution, and the other was used for the introduction of hydrazine monohydrate (0.1 mL, 1.96 mmol). A water bath was used to control the temperature of the reaction solution at 50 °C. The gas released during the reaction was passed through a HCl solution (1.0 M) before it was measured volumetrically. The selectivity toward H_2 generation (X) can be calculated using eq 3.

$$X = (3\lambda - 1)/8[\lambda = n(H_2 + N_2)/n(H_2NNH_2)] \quad (3)$$

The temperatures were varied from 25 to 60 °C, to obtain the activation energy (E_a), (catalyst = 0.100 g; $N_2H_4{\cdot}H_2O$ = 0.1 mL). Sets of experiments were performed for comparison. The $Ni_{88}Pt_{12}$@MIL-101 sample exposed in the air for 1 d before decomposition of hydrazine. Ni@MIL-101 and Pt@MIL-101 were performed in the same way as $Ni_{88}Pt_{12}$@MIL-101, and a physical mixture of 88% Ni@MIL-101 and 12% Pt@MIL-101 is used for testing the catalytic in hydrazine dehydrogenation.

Characterization. The morphologies and sizes of the samples were observed by using a Tecnai G20 U-Twin transmission electron microscope (TEM) equipped with an energy dispersive X-ray detector (EDX) at an acceleration voltage of 200 kV. Powder X-ray diffraction (XRD) patterns were measured by a Bruker D8-Advance X-ray diffractometer/PANalytical X'Pert Pro X-ray diffractometer using Cu Ka radiation source (λ = 0.154 178 nm) with a velocity of 1° min^{-1}. X-ray photoelectron spectroscopy (XPS) measurement was performed with a Kratos XSAM 800 spectrophotometer. The surface area measurements were performed with N_2 adsorption/desorption isotherms at liquid nitrogen temperature (77 K) after dehydration under vacuum at 150 °C for 12 h using Quantachrome NOVA 4200e. The inductively coupled plasma-atomic emission spectroscopy (ICP-AES) was performed on IRIS Intrepid II XSP (Thermo Fisher

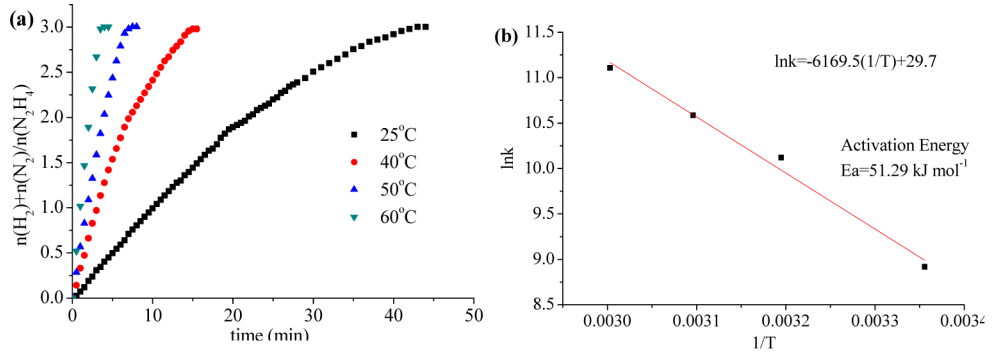

Figure 8. (a) Time course plots for hydrogen generation by the decomposition of hydrazine by $Ni_{88}Pt_{12}$@MIL-101 at 25, 40, 50, and 60 °C. (b) Plot of ln k vs $1/T$ during the hydrazine decomposition over $Ni_{88}Pt_{12}$@MIL-101 at different temperatures.

dx.doi.org/10.1021/ic5010352 | Inorg. Chem. 2014, 53, 10122−10128

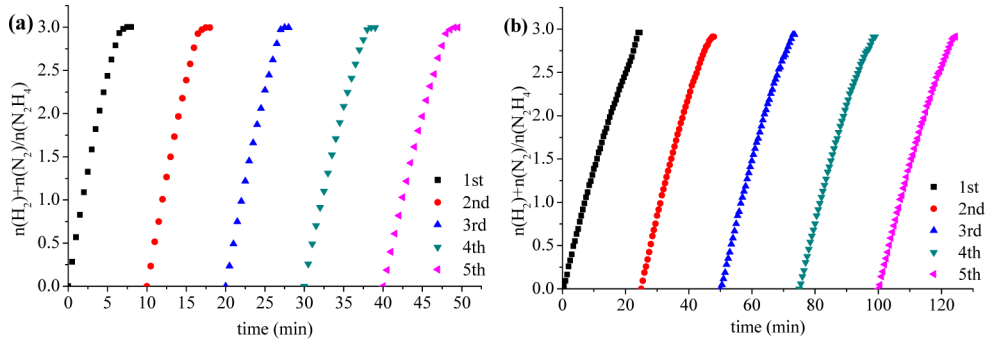

Figure 9. Durability test of (a) $Ni_{88}Pt_{12}$@MIL-101 and (b) $Ni_{97}Pt_3$@MIL-101 for decomposition of aqueous solution of hydrazine in aqueous NaOH solution (0.5 M) at 50 °C (catalyst =0.100 g; $N_2H_4{\cdot}H_2O$ = 0.1 mL). Additional aliquots of hydrazine monohydrate were subsequently introduced into the reaction vessel after the completion of the last runs.

Scientific, USA). Mass spectra (MS) of the generated gases were collected by using a Ametek Dycor mass spectrometer under Ar atmosphere.

AUTHOR INFORMATION

Corresponding Author

*Tel: (+86) 2768752366. E-mail: wluo@whu.edu.cn.

Notes

The authors declare no competing financial interest.

ACKNOWLEDGMENTS

This work was financially supported by the National Natural Science Foundation of China (21201134), the Natural Science Foundation of Jiangsu Province (BK20130370), the Natural Science Foundation of Hubei Province (2013CFB288), Ministry of Science and Technology of China (2011YQ12003504), and Large-Scale Instrument and Equipment Sharing Foundation of Wuhan University.

REFERENCES

(1) Zhao, M. Q.; Zhang, Q.; Zhang, W.; Huang, J. Q.; Zhang, Y. H.; Su, D. S.; Wei, F. *J. Am. Chem. Soc.* **2010**, *132*, 14739−14741.
(2) Wu, W. T.; Zhou, T.; Zhou, S. Q. *Chem. Mater.* **2009**, *21*, 2851−2861.
(3) Brault, P.; Caillard, A.; Baranton, S.; Mougenot, M.; Cuynet, S.; Coutanceau, C. *ChemSusChem* **2013**, *6*, 1168−1171.
(4) Cui, C. H.; Yu, S. H. *Acc. Chem. Res.* **2013**, *46*, 1427−1437.
(5) Singh, A. K.; Xu, Q. *ChemCatChem* **2013**, *5*, 652−676.
(6) Cuenya, B. R. *Acc. Chem. Res.* **2013**, *46*, 1682−1691.
(7) Balanta, A.; Godard, C.; Claver, C. *Chem. Soc. Rev.* **2011**, *40*, 4973−4985.
(8) Qian, K.; Sun, H. X.; Huang, W. X.; Fang, J.; Lv, S. S.; He, B.; Jiang, Z. Q.; Wei, S. Q. *Chem.—Eur. J.* **2008**, *14*, 10595−10602.
(9) Liu, X. Y.; Wang, A. Q.; Wang, X. D.; Mou, C.-Y.; Zhang, T. *Chem. Commun.* **2008**, 3187−3189.
(10) Chiang, C.-W.; Wang, A. Q.; Wan, B.-Z.; Mou, C.-Y. *J. Phys. Chem. B* **2005**, *109*, 18042−18047.
(11) Tosheva, L.; Valtchev, V. P. *Chem. Mater.* **2005**, *17*, 2494−2513.
(12) Wang, X.; Liu, D. P.; Song, S. Y.; Zhang, H. J. *J. Am. Chem. Soc.* **2013**, *135*, 15864−15872.
(13) Shi, F.; Zhang, Q. H.; Ma, Y. B.; He, Y. D.; Deng, Y. Q. *J. Am. Chem. Soc.* **2005**, *127*, 4182−4183.
(14) Khajeh, M.; Laurent, S.; Dastafkan, K. *Chem. Rev.* **2013**, *113*, 7728−7768.
(15) Guo, S. J.; Zhang, S.; Sun, S. H. *Angew. Chem., Int. Ed.* **2013**, *52*, 8526−8544.
(16) Xue, D. X.; Cairns, A. J.; Belmabkhout, Y.; Wojtas, L.; Liu, Y. L.; Alkordi, M. H.; Eddaoudi, M. *J. Am. Chem. Soc.* **2013**, *135*, 7660−7667.
(17) Keskin, S.; van Heest, T. M.; Sholl, D. S. *ChemSusChem* **2010**, *3*, 879−891.
(18) Wriedt, M.; Sculley, J. P.; Yakovenko, A. A.; Ma, Y. G.; Halder, G. J.; Balbuena, P. B.; Zhou, H. C. *Angew. Chem., Int. Ed.* **2012**, *51*, 9804−9808.
(19) Couck, S.; Gobechiya, E.; Serra-Crespo, C. E. A. P.; Juan-Alcañiz, J.; Joaristi, A. M.; Stavitski, E.; Gascon, J.; Kapteijn, F.; Baron, G. V.; Denayer, J. F. M. *ChemSusChem* **2012**, *5*, 740−750.
(20) Wang, Y.; Yang, J.; Liu, Y. Y.; Ma, J. F. *Chem.—Eur. J.* **2013**, *19*, 14591−14599.
(21) Liédana, N.; Galve, A.; Rubio, C.; Téllez, C.; Coronas, J. *ACS Appl. Mater. Interfaces* **2012**, *4*, 5016−5021.
(22) Kreno, L. E.; Leong, K.; Farha, O. K.; Allendorf, M.; Van Duyne, R. P.; Hupp, J. T. *Chem. Rev.* **2012**, *112*, 1105−1125.
(23) Shekhah, O.; Liu, J.; Fischer, R. A.; Wöll, C. *Chem. Soc. Rev.* **2011**, *40*, 1081−1106.
(24) Coronado, E.; Espallargas, G. M. *Chem. Soc. Rev.* **2013**, *42*, 1525−1539.
(25) Ricco, R.; Malfatti, L.; Takahashi, M.; Hill, A. J.; Falcaro, P. *J. Mater. Chem. A* **2013**, *1*, 13033−13045.
(26) Yoon, M.; Srirambalaji, R.; Kim, K. *Chem. Rev.* **2012**, *112*, 1196−1231.
(27) Zhang, Y. M.; Degirmenci, V.; Li, C.; Hensen, E. J. M. *ChemSusChem* **2011**, *4*, 59−64.
(28) Moon, H. R.; Limb, D.-W.; Suh, M. P. *Chem. Soc. Rev.* **2013**, *42*, 1807−1824.
(29) Zhao, M. T.; Deng, K.; He, L. C.; Liu, Y.; Li, G. D.; Zhao, H. J.; Tang, Z. Y. *J. Am. Chem. Soc.* **2014**, *136*, 1738−1741.
(30) He, L. C.; Liu, Y.; Liu, J. Z.; Xiong, Y. S.; Zheng, J. Z.; Liu, Y. L.; Tang, Z. Y. *Angew. Chem., Int. Ed.* **2013**, *52*, 3741−3745.
(31) Liu, Y. L.; Tang, Z. Y. *Adv. Mater.* **2013**, *25*, 5819−5825.
(32) Gu, X. J.; Lu, Z. H.; Jiang, H. L.; Akita, T.; Xu, Q. *J. Am. Chem. Soc.* **2011**, *133*, 11822−11825.
(33) Long, J. L.; Liu, H. L.; Wu, S. J.; Liao, S. J.; Li, Y. W. *ACS Catal.* **2013**, *3*, 647−654.
(34) Singh, A. K.; Xu, Q. *ChemCatChem.* **2013**, *5*, 3000−3004.
(35) Eberle, U.; Felderhoff, M.; Schüth, F. *Angew. Chem., Int. Ed.* **2009**, *48*, 6608−6630.
(36) Graetz, J. *Chem. Soc. Rev.* **2009**, *38*, 73−82.
(37) Zhao, D.; Yuan, D. Q.; Zhou, H. C. *Energy Environ. Sci.* **2008**, *1*, 222−235.
(38) Suh, M. P.; Park, H. J.; Prasad, T. K.; Lim, D.-W. *Chem. Rev.* **2012**, *112*, 782−835.
(39) Stephens, F. H.; Pons, V.; Baker, R. T. *Dalton Trans.* **2007**, 2613−2626.
(40) Luo, W.; Campbell, P. G.; Zakharov, L. N.; Liu, S. Y. *J. Am. Chem. Soc.* **2011**, *133*, 19326−19329.
(41) Singh, S. K.; Zhang, X. B.; Xu, Q. *J. Am. Chem. Soc.* **2009**, *131*, 9894−9895.
(42) He, L.; Huang, Y. Q.; Wang, A. Q.; Liu, Y.; Liu, X. Y.; Chen, X. W.; Delgado, J. J.; Wang, X. D.; Zhang, T. *J. Catal.* **2013**, *298*, 1−9.

(43) Aranishi, K.; Singh, A. K.; Xu, Q. *ChemCatChem* **2013**, *5*, 2248−2252.
(44) Yadav, M.; Xu, Q. *Energy Environ. Sci.* **2012**, *5*, 9698−9725.
(45) He, L.; Huang, Y. Q.; Wang, A. Q.; Wang, X. D.; Zhang, T. *AIChE J.* **2013**, *59*, 4297−4302.
(46) Zhang, J. J.; Kang, Q.; Yang, Z. Q.; Dai, H. B.; Zhuang, D. W.; Wang, P. *J. Mater. Chem. A* **2013**, *1*, 11623−11628.
(47) Wang, H. L.; Yan, J. M.; Wang, Z. L.; O, S. −II; Jiang, Q. *J. Mater. Chem. A* **2013**, *1*, 14957−14962.
(48) Singh, S. K.; Xu, Q. *J. Am. Chem. Soc.* **2009**, *131*, 18032−18033.
(49) Singh, S. K.; Singh, A. K.; Aranishi, K.; Xu, Q. *J. Am. Chem. Soc.* **2011**, *133*, 19638−19641.
(50) Singh, S. K.; Xu, Q. *Inorg. Chem.* **2010**, *49*, 6148−6152.
(51) Tong, D. G.; Chu, W.; Wu, P.; Gu, G. F.; Zhang, L. *J. Mater. Chem. A* **2013**, *1*, 358−366.
(52) Singh, S. K.; Iizuka, Y.; Xu, Q. *Int. J. Hydrogen Energy* **2011**, *36*, 11794−11801.
(53) Singh, A. K.; Yadav, M.; Aranishi, K.; Xu, Q. *Int. J. Hydrogen Energy* **2011**, *36*, 18915−18919.
(54) Wang, J.; Zhang, X. B.; Wang, Z. L.; Wang, L. M.; Zhang, Y. *Energy Environ. Sci.* **2012**, *5*, 6885−6888.
(55) Férey, G.; Mellot-Draznieks, C.; Serre, C.; Millange, F.; Dutour, J.; Surblé, S.; Margiolaki, I. *Science* **2005**, *309*, 2040−2042.
(56) Hermannsdörfer, J.; Kempe, R. *Chem.—Eur. J.* **2011**, *17*, 8071−8077.
(57) Li, H.; Zhu, Z. H.; Zhang, F.; Xie, S. H.; Li, H. X.; Li, P.; Zhou, X. G. *ACS Catal.* **2011**, *1*, 1604−1612.
(58) Singh, S. K.; Lu, Z. H.; Xu, Q. *Eur. J. Inorg. Chem.* **2011**, 2232−2237.
(59) Gao, W.; Li, C. M.; Chen, H.; Wu, M.; He, S.; Wei, M.; Evans, D. G.; Duan, X. *Green Chem.* **2013**, *16*, 1560−1568.
(60) Singh, S. K.; Xu, Q. *Chem. Commun.* **2010**, *46*, 6545−6547.